

# Plasma wakefield generation and electron acceleration in a self-modulated laser wakefield accelerator experiment\*

A. Ting,<sup>†</sup> C. I. Moore,<sup>a)</sup> K. Krushelnick,<sup>b)</sup> C. Manka, E. Esarey, P. Sprangle, R. Hubbard, H. R. Burris, R. Fischer, and M. Baine<sup>c)</sup>

Plasma Physics Division, Naval Research Laboratory, Washington, D.C. 20375

(Received 11 November 1996; accepted 28 January 1997)

A self-modulated laser wakefield accelerator (SM-LWFA) experiment was performed at the Naval Research Laboratory. Large amplitude plasma wakefields produced by a sub-picosecond, high intensity laser pulse ( $7 \times 10^{18}$  W/cm<sup>2</sup>) in an underdense plasma ( $n_e \approx 10^{19}$  cm<sup>-3</sup>) were measured with a pump-probe coherent Thomson scattering (CTS) technique to last for less than 5 ps, consistent with the decay of large amplitude plasma waves due to the modulational instability. A plasma channel was observed to form in the wake of the pump laser pulse, and its evolution was measured with the pump-probe CTS diagnostic. The trailing probe laser pulse was observed to be guided by this channel for about 20 Rayleigh lengths. High energy electrons (up to 30 MeV) have been measured using an electro-magnetic spectrometer, with the energy spectra and divergence of lower energy (up to 4 MeV) electrons obtained using photographic films. Highly nonlinear plasma waves were also detected using forward Raman scattering diagnostics and were observed to correlate with the electron signals. Simulations of self-trapping of plasma electrons from the interaction of the laser wakefield with the slow plasma wave generated by Raman backscattering are also presented. © 1997 American Institute of Physics. [S1070-664X(97)94305-6]

## I. INTRODUCTION

Significant progress has been made in recent years<sup>1</sup> using laser-produced plasmas as a medium for accelerating electrons to high energies. In the Laser Wakefield Accelerator (LWFA),<sup>2</sup> a high intensity laser pulse is focused into an underdense plasma with a pulse duration,  $\tau_L$ , close to the electron plasma period (i.e.,  $\tau_L \sim 2\pi/\omega_{pe}$  where  $\omega_{pe}$  is the electron plasma frequency). Large amplitude plasma waves (wakefields) are generated with strong longitudinal electric fields and relativistic phase velocities which are capable of accelerating injected electrons. For laser powers,  $P$ , approaching or exceeding the relativistic self-focusing threshold (i.e.,  $P_c > 17 (\omega_0/\omega_{pe})^2$  GW; where  $\omega_0$  is the laser frequency), it is not necessary to match the pulse duration to the plasma period. At laser powers for which  $P \geq P_c$  and  $\tau_L > 2\pi/\omega_{pe}$ , the laser envelope undergoes an instability and becomes “self-modulated” at the plasma frequency.<sup>3,4</sup> This effect resonantly enhances the creation of wakefields and allows use of higher electron densities and generates stronger accelerating fields.<sup>5</sup> Recent experiments in this self-modulated laser wakefield accelerator (SM-LWFA) regime have measured the production of high energy electrons where the source of accelerated particles was either background electrons from the target plasma<sup>6-9</sup> or electrons injected into the interaction region from an adjacent laser-produced plasma.<sup>10</sup> Direct observations of wakefields in the conventional LWFA configuration were recently reported us-

ing interferometric techniques, in which the spatial and temporal wave forms of the wakefield were measured.<sup>11</sup>

In order to obtain high final energies of the accelerated electrons in a LWFA, it is necessary that the laser propagates long distances at high intensity in the plasma. This implies that the laser pulse must be “guided” for distances significantly greater than the vacuum diffraction length (Rayleigh range), which is typically less than a hundred microns if the beam is tightly focused. Guiding of intense laser pulses in plasmas has been demonstrated by a variety of mechanisms. Laser light with intensities of up to  $5 \times 10^{15}$  W cm<sup>2</sup> has been channeled in a 3 cm waveguide structure created by the hydrodynamic expansion of a preformed plasma<sup>12</sup> and intensities of  $10^{16}$  W cm<sup>2</sup> have been propagated for up to 3 cm in vacuum using glass capillary waveguides.<sup>13</sup> In addition, a preformed plasma generated by a capillary discharge has been used to guide  $10^{16}$  W/cm<sup>2</sup> laser pulses.<sup>14</sup> For laser pulses above the critical power for relativistic optical guiding,  $P_c$ , self-channeling of laser pulses in plasmas has been experimentally observed<sup>15,16</sup> and has been the subject of extensive theoretical examination.<sup>1,3-5,17,18</sup> Self-focusing of intense laser pulses in plasmas can also be enhanced by the expulsion of plasma electrons (cavitation) produced by the extreme ponderomotive force of a focused laser pulse.<sup>18</sup>

Large amplitude relativistic plasma waves generated in the SM-LWFA have axial accelerating electric fields with extremely high gradients ( $\sim 100$  GeV/m).<sup>3,6</sup> The phase velocity of the plasma wave is approximately equal to the group velocity of the laser pulse ( $\sim c$ ), and hence, these plasma waves are very suitable for high energy particle acceleration. Nakajima *et al.*<sup>10</sup> have observed high energy electrons ( $\sim 17$  MeV) being accelerated in a SM-LWFA experiment where  $\sim 1$  MeV electrons were injected. Coverdale *et al.*<sup>6</sup> and Umstadter *et al.*<sup>8</sup> have observed 2 and 5 MeV

\*Paper 4IB2, Bull. Am. Phys. Soc. **41**, 1474 (1996).

<sup>†</sup>Invited speaker.

<sup>a)</sup>National Research Council/NRL Postdoctoral Fellow.

<sup>b)</sup>Laboratory for Plasma Studies, Cornell University, Ithaca, New York 14853.

<sup>c)</sup>University of California at San Diego, La Jolla, California 92093.

accelerated electrons, respectively from self-trapping of background plasma electrons. Recent SM-LWFA experiments by Modena *et al.*<sup>7</sup> used a 25 TW laser pulse to drive nonlinear wakefield plasma waves in a helium plasma resulting in the capture and acceleration of background plasma electrons to 44 MeV.<sup>7</sup> Their experiments showed a broadening of the anti-Stokes lines in the forward Raman scattering (FRS) spectrum concurrent with the onset of high energy electron production at approximately 7 TW. This broadening and high energy electron production was attributed to the onset of wave breaking.<sup>7</sup>

The wakefields in a LWFA cannot normally accelerate background plasma electrons directly because the phase velocity of the wakefield is near the velocity of light. Injection of an electron beam from an rf gun at an energy of several MeV is usually required. However, recent LWFA experiments at the Naval Research Laboratory (NRL) and elsewhere<sup>6–9</sup> have detected high energy electrons even in situations where there is no injected electron beam. Mechanisms for self-trapping of background plasma electrons<sup>7,19,20</sup> and the trapping of electrons by the interaction of external laser pulses<sup>21,22</sup> with the wakefields have been proposed which offer the possibility of “injectorless” acceleration.

In this paper, we present results of recent SM-LWFA experiments performed at the Naval Research Laboratory. We discuss the experimental diagnostics that monitor pump–probe Thomson forward and side scattered radiation in Sec. II. Time evolution of the relativistic plasma wakefield was measured and is discussed in Sec. III. The formation of a plasma channel by the pump pulse and the subsequent guiding of the probe pulse are discussed in Sec. IV. High energy electron measurements and their correlation with nonlinear wakefield amplitudes are discussed in Sec. V. Simulations that demonstrate the trapping and acceleration of background plasma electrons by the wakefield are discussed in Sec. VI. These experimental and theoretical results on the SM-LWFA are summarized in Sec. VII.

## II. EXPERIMENT

These experiments were performed with the NRL tabletop terawatt laser system which is a Ti:Sapphire/Nd:Glass system ( $\lambda = 1.054 \mu\text{m}$ ) which uses chirped pulse amplification<sup>23</sup> to achieve the high powers necessary for experiments in the self-modulated regime. In these experiments, the pump laser pulse had a typical duration of 400 fs and an energy of 800–1200 mJ ( $P = 2–3 \text{ TW}$ ). The contrast (i.e., the ratio of the prepulse intensity to that at the peak of the laser pulse) was measured to be  $10^{-6}$ . The beam was focused with an  $f/3$  off-axis parabolic mirror. The measured focal spot radius of  $r_0 \sim 4.5 \mu\text{m}$  corresponds to a vacuum Rayleigh length of  $Z_R = \pi r_0^2 / \lambda \sim 60 \mu\text{m}$ . At  $P = 2 \text{ TW}$ , the peak focused intensity is  $7 \times 10^{18} \text{ W cm}^2$ . This laser could be operated with a repetition rate of about 1 shot/3 min at the maximum power used in these experiments.

To reduce ionization induced defocusing effects<sup>24</sup> which may occur during interactions in static-filled gas chambers, a jet of helium or hydrogen gas was produced in a vacuum chamber by operation of a pulsed gas valve and nozzle. We

measured the plasma electron density by recording the frequency shift of stimulated Raman backscattered light produced during interactions at moderate intensity ( $10^{16} \text{ W cm}^2$ ). This shift, the Bohm–Gross frequency, is approximately the electron plasma frequency,  $\omega_{pe}$ , at low electron temperatures and is related to the plasma electron density (i.e.,  $\omega_{pe} = (4\pi n_e e^2 / m_e)^{1/2}$ ). For plenum pressures of 200 psi the plasma electron density was found to be  $10^{19} \text{ cm}^{-3}$ . For a plasma density of  $n_0 \sim 10^{19} \text{ cm}^{-3}$ , the critical power is  $P_c \sim 1.8 \text{ TW}$ , and the plasma wavelength is  $\lambda_{pe} = 2\pi c / \omega_{pe} \sim 10 \mu\text{m}$ . Hence,  $P \geq P_c$  and  $c\tau_L \sim 12\lambda_{pe}$ , which are necessary for operation in the SM-LWFA regime. The gas jet was measured to have a diameter of approximately 3 mm with a central uniform region of about 2 mm. The scalelength for the density gradient at the edges of the jet was about 0.5 mm. During our experiments, the high intensity laser beam was focused in the front portion of the gas jet to minimize any possible effects of ionization induced refraction.

A pump–probe experimental arrangement was used to monitor the temporal characteristics of the high intensity laser produced plasma, as shown in Fig. 1. Approximately 10% of the main beam was split off by a pellicle for use as a probe pulse and was subsequently frequency doubled (to 527 nm) by a 1 cm thick KD\*P crystal. For 800 mJ pump pulses the probe pulse energy was 10 mJ. The maximum broadening of the probe pulse length from passage through the doubling crystal will result in a pulse duration,  $\tau_{L,p} < 1 \text{ ps}$ . This provides the intrinsic temporal resolution for our experiment. Since  $c\tau_{L,p} \gg \lambda_{pe}$  in these experiments, the probe pulse efficiently sampled the plasma waves it measured. This is in contrast to optical interferometric techniques<sup>11</sup> which require much shorter probe pulses such that  $c\tau_{L,p} < \lambda_{pe}$ . The probe pulse traverses a delay line and then is recombined with the main beam before being focused into the plasma created by the pump pulse. This delay line can be adjusted to vary the timing between the two pulses. The paths of the two beams were overlapped by alignment to a series of apertures prior to the focusing optic (an off-axis parabolic mirror which focused the probe beam at  $f/6$  and the pump beam at  $f/3$ ) and by observation of scattered light in the focal region. In some experiments, small offset angles ( $\sim 10^\circ$ ) between the pump and probe beams were obtained by displacing the probe beam laterally on the final focusing mirror.

Coarse temporal synchronization of pump and probe pulses was achieved using a streak camera with better than 4 ps resolution. Fine temporal synchronization was attained by measuring the probe frequency after passage through the interaction region. If the probe pulse travels ahead of the pump, it ionizes the gas and generates a blue shift in the spectrum.<sup>25</sup> Otherwise, the frequency is unshifted. This effect is easily observed and provides a measurement of the temporal overlap to within 1 ps.

Directly forward scattered light was recollimated by a parabolic mirror similar to that used to focus the beam, while radiation scattered at off-axis angles was collected by a single lens and imaged onto the slit of a 0.25 m Czerny–Turner spectrometer which operated in the visible and near infrared. The interaction was also monitored by transversely

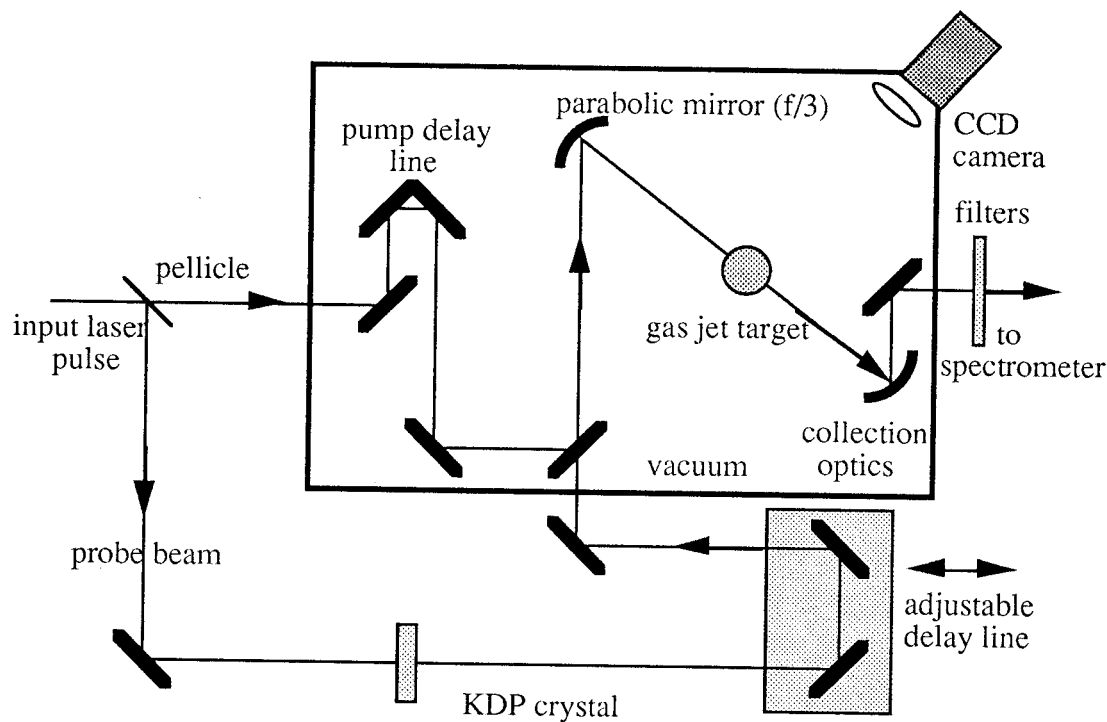


FIG. 1. Schematic of Thomson scattering experimental setup.

imaging Thomson scattered laser light onto a charge coupled device (CCD) array positioned at  $90^\circ$  from the axis of propagation.

Electron measurements and forward Raman scattering measurements were performed using the experimental setup shown in Fig. 2. Forward Raman scattered laser light at  $40^\circ$  to the laser axis was imaged on the entrance slit of a spectrometer to measure the relative wakefield amplitude and linearity. An inline spectrometer configuration measured the energy distribution of electrons accelerated from the background plasma. The electron spectrometer consisted of an electromagnet for electron deflection and a plastic scintillator directly coupled to a photomultiplier tube (PMT) for electron detection. The electromagnet used a 0–2500 G magnetic field in a field region 5.5 cm long. Graphite and carbon shielding were arranged with a small gap centered on the laser axis which allowed only high energy electrons with less than an  $8^\circ$  deflection in the magnet to strike the scintillator. Electrons with lower energies were deflected more than  $8^\circ$  and dumped in a graphite block to minimize x-ray production. This inline spectrometer configuration therefore detects all electrons above a cutoff energy which is determined by the magnetic field strength and the maximum acceptance angle of the gap in the shielding ( $8^\circ$ ).

Kodak DEF x-ray film (direct exposure x-ray film) was also used for electron detections in two configurations. In the first configuration, the electromagnet was used to disperse the electrons on the film and generate a continuous energy spectrum. In the second configuration, the magnet was removed and a thin sheet of lead was placed over the film to block low energy electrons ( $<1$  MeV). The profile of high energy electrons is then recorded on the film. In both con-

figurations the film was wrapped in  $50\ \mu\text{m}$  of aluminum foil to block laser and ambient light from exposing the film.

### III. TIME EVOLUTION OF PLASMA WAKEFIELDS IN THE SM-LWFA

Coherent Thomson scattering (CTS) of a picosecond probe laser pulse was used to measure the temporal behavior of self-modulated wakefields in the SM-LWFA.<sup>26</sup> Coherently scattered light has a wave vector  $\mathbf{k}_{sc}$  and a frequency  $\omega_{sc}$  that satisfy the Bragg scattering conditions of frequency and wave number matching. For electron plasma waves with  $\omega_{pe}$  and  $\mathbf{k}_{pe}$ , the conditions require  $\omega_{sc} = \omega_1 \pm \omega_{pe}$  and  $\mathbf{k}_{sc} = \mathbf{k}_1 \pm \mathbf{k}_{pe}$ , where  $\omega_1$  is the frequency and  $\mathbf{k}_1$  is the wave vector of the probe laser. The plasma wakefields in an SM-LWFA have relativistic phase velocities,  $v_\phi \sim c$ , such that they are capable of accelerating electrons to high energies. For correct matching of  $\mathbf{k}$  vectors, both the probe and the Thomson scattered light must therefore propagate in the same direction as the relativistic plasma wave (i.e., pump, probe, and scattered light propagating collinearly). Unscattered light from the pump beam was attenuated by an infrared absorption filter after the interaction region. The majority of the 527 nm probe light was not scattered and was blocked before the slit of the spectrometer by a notch filter in the beam path. However, the Thomson scattered electron plasma satellites of the probe light, which are shifted by  $\omega_{pe}$  ( $\Delta\lambda_{\text{Stokes}} \approx 23$  nm,  $\Delta\lambda_{\text{anti-Stokes}} \approx 21$  nm for a plasma density of  $7 \times 10^{18}$  cm $^{-3}$  as in Fig. 3), are positioned beyond the edges of the absorption band of the notch filter and hence will be detected by the spectrometer. The principal result in this configuration was the observation of these plasma satel-

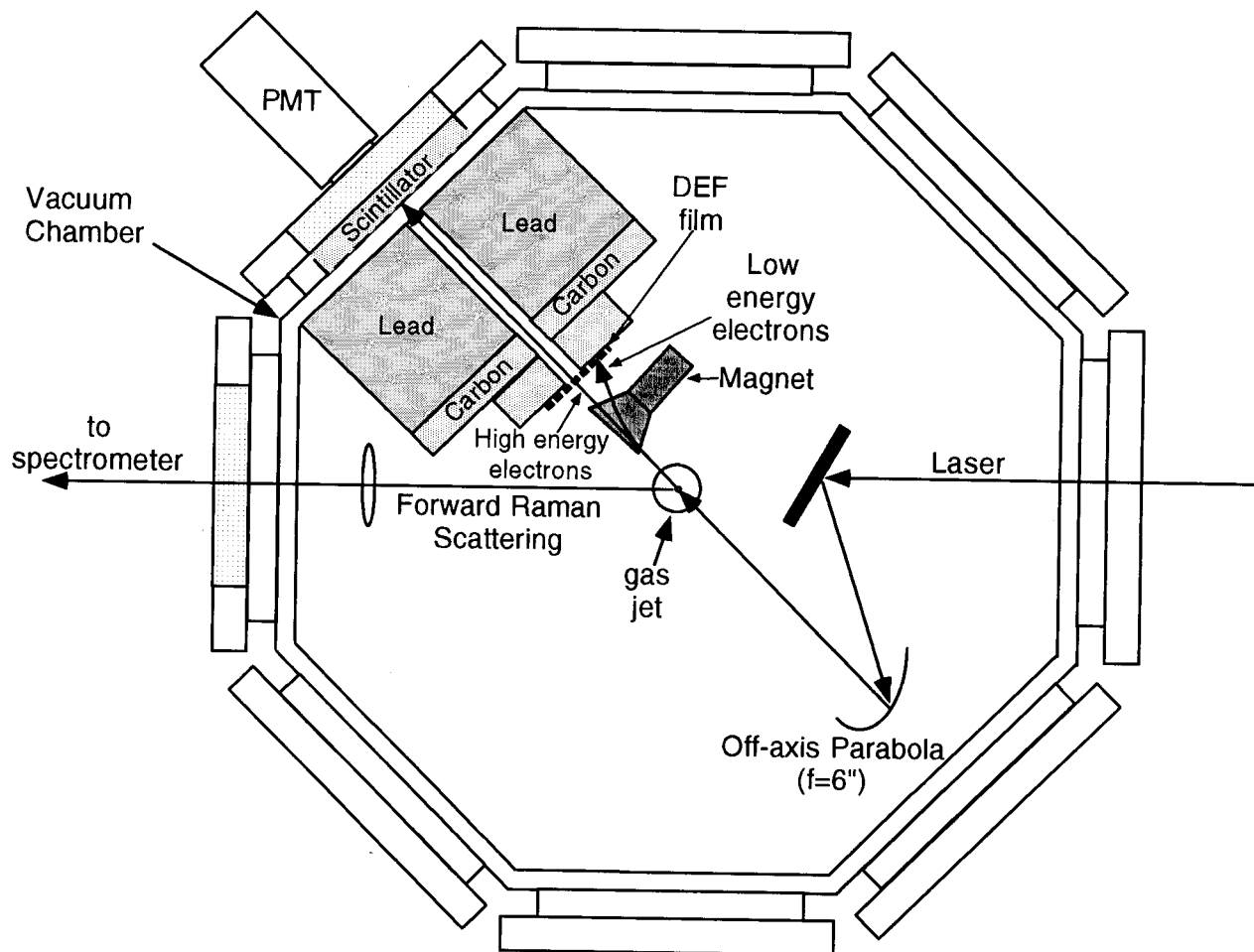


FIG. 2. Schematic of experimental setup for accelerated electron measurements.

lites for about 5 ps after passage of the pump laser. Figure 3 shows a full width at half maximum (FWHM) of  $\sim 2$  ps which is similar to the wakefield lifetime measured by similar techniques reported in Ref. 27. As shown in the insert in

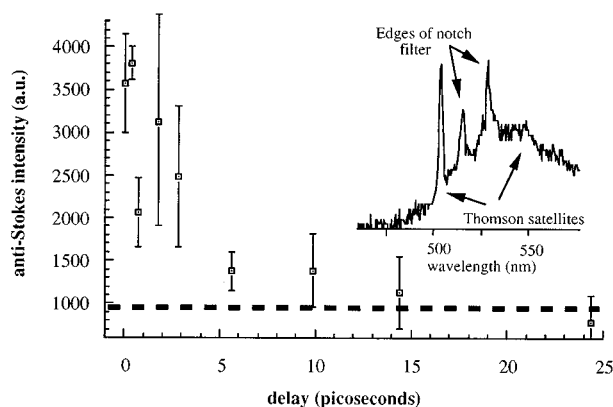


FIG. 3. Evolution of electron satellites from zero-degree coherent Thomson scattering. The background level is shown by the dashed line. Data are not shown for pump-probe delay times less than zero since blueshifting of the probe laser spectrum saturates the detector for early times. Insert is a typical spectrum (Stokes at 506 nm, anti-Stokes at 550 nm).

Fig. 3, the anti-Stokes line was typically more intense than the Stokes line, perhaps indicating that the  $\mathbf{k}$ -vectors of the electron plasma waves in the wakefield are primarily in the forward direction.<sup>28</sup> These measurements confirmed the generation of wakefields with  $v_\phi \sim c$ .<sup>29</sup>

The ratio of the total scattered signal intensity to the probe intensity is given by,<sup>30</sup>  $I_s/I_1 \approx 2.5(\delta n L_z/n_{cr}\lambda_1)^2$ , where  $n_{cr}$  is the critical density for the probe wavelength ( $4 \times 10^{21} \text{ cm}^{-3}$ ),  $\lambda_1$  is the probe wavelength,  $L_z$  is probe-plasma interaction length (the confocal parameter of the probe laser,  $\sim 200 \mu\text{m}$ ) and  $\delta n$  is the density perturbation of the wave. We estimate the ratio  $(I_s/I_1)$  to be  $10^{-3 \pm 1}$  for scattering into the electron plasma satellites. This implies that the amplitude of plasma waves encountered by the probe pulse ( $\delta n/n_0$ , where  $n_0$  is the ambient density) was up to  $10^{-1}$ .

The wakefields generated in these experiments are highly three-dimensional due to the tight focusing of the pump laser. This causes a strong radial profile of the wakefield which implies that the scattering plasma waves have significant  $\mathbf{k}_\perp$  components ( $\sim 2\pi/r_0$ ,  $r_0$  being the pump laser focal spot radius) and lower phase velocities. These lower phase velocity plasma waves couple more readily with the probe laser to scatter in the near forward directions. In fact, a

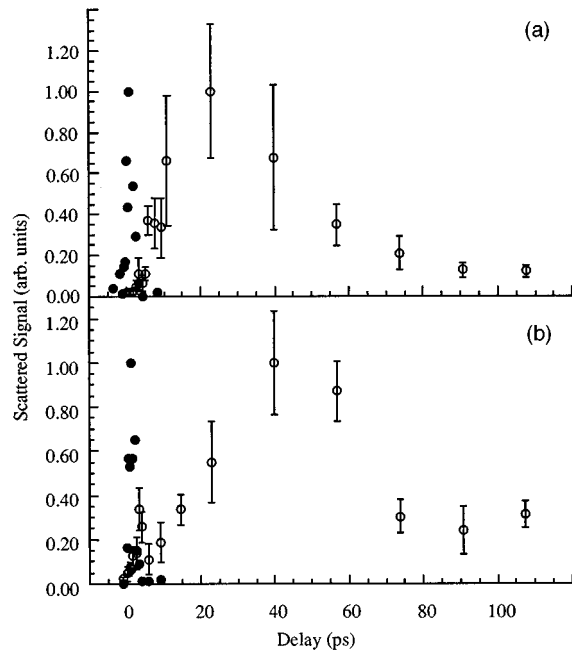


FIG. 4. Evolution of Thomson scattered spectrum at 30° scattering angle relative to the pump laser but 20° relative to the probe: (a) hydrogen, (b) helium. Open circles are normalized values of the central peak in the scattered spectrum and closed circles are the normalized value of the first order Stokes satellite.

10° tilt between the pump and probe lasers by displacing the probe laser on the focusing parabolic mirror (while maintaining the 30° angle to the pump for the scattered light) gave a better signal to noise ratio without changes to the general behavior of the scattered signal. These electron satellite emission lasted for about 5–7 ps in both hydrogen and helium, as shown by the closed circles in Fig. 4, similar to that observed in the directly forward direction.

A dramatic rise in the central peak of the Thomson scattered spectrum was also observed at  $t > 10$  ps, which correlates to the decline of the electron plasma sidebands. We believe this central peak is due to coherent Thomson scattering from ion acoustic waves since both a strong dependence on the polarization of the probe beam and a dependence of its intensity on  $n_e^2$  were observed. The open circles in Fig. 4 show that the amplitude of the central scattered peak reached a maximum at  $\Delta t \approx 25$  ps after the main pulse for hydrogen and at  $\Delta t \approx 40$  ps for helium. We believe this is due to the turbulent decay of the forward going large amplitude plasma waves into ion acoustic waves through mechanisms such as the modulational instability.

For moderate temperatures ( $T_e < 1$  keV), a Langmuir wave is subject to the modulation instability (MI),<sup>31</sup> in which a plasma wave ( $\omega_p, \mathbf{k}_p$ ) decays into a low-frequency ion wave ( $\omega_i, \mathbf{k}_i$ ) and two daughter electron plasma waves ( $\omega_p \pm \omega_i, \mathbf{k}_p \pm \mathbf{k}_i$ ), where typically  $k_i \gg k_p$ . Ion waves generated by MI have been observed coincident with plasma waves in experiments on the plasma beat wave accelerator.<sup>32</sup> In these experiments, the plasma wave is simultaneously driven by the long duration laser pulses ( $\sim 150$  ps) while decaying via MI. In SM-LWFA experiments, on the other hand, the plasma waves are first generated very rapidly ( $< 1$  ps) and

then decay into ion waves in the region behind the laser pulse. Collisional damping of the wakefield can be neglected, since for electrons oscillating in a  $\delta n/n_0 \sim 0.1$  plasma wave, the electron-ion collision time is long (typically  $\sim 300$  ps).

The linear growth rate<sup>31</sup> of MI depends on the parameter  $v_L/v_{te} = 23(\delta n/n_0)T_e^{-1/2}$ , where  $T_e$  is the electron temperature in keV,  $v_L$  is the electron quiver velocity in the Langmuir wave and  $v_{te}$  is the electron thermal velocity. MI occurs in the strong field limit when  $v_L/v_{te} > (\omega_{pe}/\omega_{pi})^{1/3}$ , where  $\omega_{pe}$  and  $\omega_{pi}$  are the plasma frequencies for the electrons and ions, respectively. Initially, if the plasma wave amplitude is large ( $\delta n/n_0 \sim 0.1$ ) and for  $T_e \sim 10$  eV, the strong field condition is satisfied such that  $v_L/v_{te} \sim 23$  and  $(\omega_{pe}/\omega_{pi})^{1/3} \sim 3$ . The maximum strong field growth rate<sup>31</sup> is approximately given by the ion plasma period ( $\gamma_{sf} \sim \omega_{pi}$ ) and the corresponding  $e$ -folding time  $\tau_{sf} = 1/\gamma_{sf}$  is short, about 0.3 ps for H<sub>2</sub> ( $2\pi/\omega_{pi} = 1.8$  ps) and about 0.4 ps for He ( $2\pi/\omega_{pi} = 2.5$  ps).

As the initial wakefield decays, however,  $\delta n/n_0$  decreases and MI transitions<sup>31</sup> to the slower growth of the weak field limit,  $v_L/v_{te} < (\omega_{pe}/\omega_{pi})^{1/3}$ , with a maximum weak field growth rate of  $\gamma_{wf} \sim 6^{-1/2}\omega_{pi}(v_L/v_{te})$ . Notice that as  $\delta n/n_0$  ( $\sim v_L/v_{te}$ ) decreases, so does the growth rate. In addition, the decay of the wakefield behind the laser pulse is likely to be accompanied by electron plasma heating, which will also decrease the growth of MI. The daughter plasma waves may also decay and hence can lead to a cascade of the wakefield energy into smaller amplitude daughter waves and drive ion waves over longer time scales. For example,  $\delta n/n_0 \sim 10^{-3}$  and  $T_e = 100$  eV give  $\tau_{wf} = 1/\gamma_{wf} \sim 8$  ps for H<sub>2</sub> (11 ps for He) which agree reasonably well with the time scales shown in Figs. 4(a) and 4(b).

#### IV. PLASMA CHANNEL FORMATION AND OPTICAL GUIDING

The temporal behavior of the central scattered peak shown in Fig. 4 may also be affected by the formation of a plasma channel. Plasma channel formation is possible because the pump laser is observed to be guided in the plasma<sup>15,16</sup> and a channel may be left in its wake.<sup>16,33</sup> The propagation of the probe pulses was monitored by imaging the Thomson scattered emission at 90° to the laser propagation direction onto a CCD through a 527 nm filter ( $\Delta\lambda = 5$  nm). When only the probe pulse was injected into the gas jet, very little Thomson scattered emission was observed even though a plasma was created. However, if both pump and probe pulses were incident simultaneously on the gas jet, a bright image of scattered probe light (527 nm) was observed in the region where the pump beam was channeling. This emission is probably caused by coherent Thomson scattering of the probe laser from ion acoustic waves generated in the turbulent decay of the large amplitude plasma waves in the wakefield of the pulse.<sup>26</sup> This emission was observed even as the temporal separation between the pump and probe laser pulses was increased by more than the laser pulsewidth (see Fig. 5). In fact, the brightness of the Thomson scattered image from the probe reached a maximum approximately 15 ps after passage of the pump pulse. Thomson scattered emis-

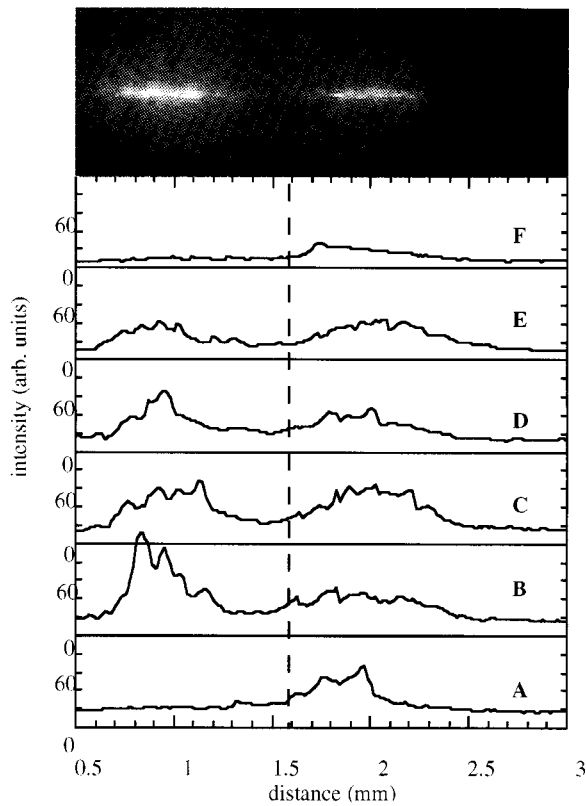


FIG. 5. Thomson scattering images of interaction of picosecond probe beam (527 nm) for various delay settings between pump and probe beam in hydrogen gas jet. (a) 0, (b) 6, (c) 14, (d) 22, (e) 30, (f) 46 ps (propagation from right to left). Typical CCD image ( $\Delta t = 19$  ps) shown at top. Dashed line indicates approximate position of vacuum focus (centered in gas jet).

sion from the probe continued for pump-probe delays of more than 40 ps before decreasing significantly.

As the delay between pump and probe pulses is changed, the observed waveguide structure also appears to change qualitatively. It is clear from Fig. 5 that for small temporal separations the Thomson emission profile of the probe light has a complex structure. However, if the delay is increased by several tens of picoseconds the Thomson scattered image appears smoother. This effect may be due to hydrodynamic motion of the plasma which can reduce nonuniformities caused by the channel production mechanism. Such motion should occur at approximately the sound speed in the plasma. The plasma temperature from similar interactions has been measured immediately after the interaction to be about  $100 \text{ eV}^{34}$  which results in a sound speed of about  $0.1 \mu\text{m/ps}$  agreeing with the time scales observed in the evolution of the Thomson scattered probe light. In addition, as the size of the plasma channel increases, the decrease in the probe light intensity could also contribute to the observed reduction in the level of Thomson emission. At large delays the observed emission near 527 nm [see Fig. 5(f)] is second harmonic light generated by the pump laser itself.<sup>35</sup> Identical experiments were performed in which helium was used as the target gas producing similar experimental results, although the characteristic channel formation time was observed to be somewhat longer due to the slower plasma sound speed.

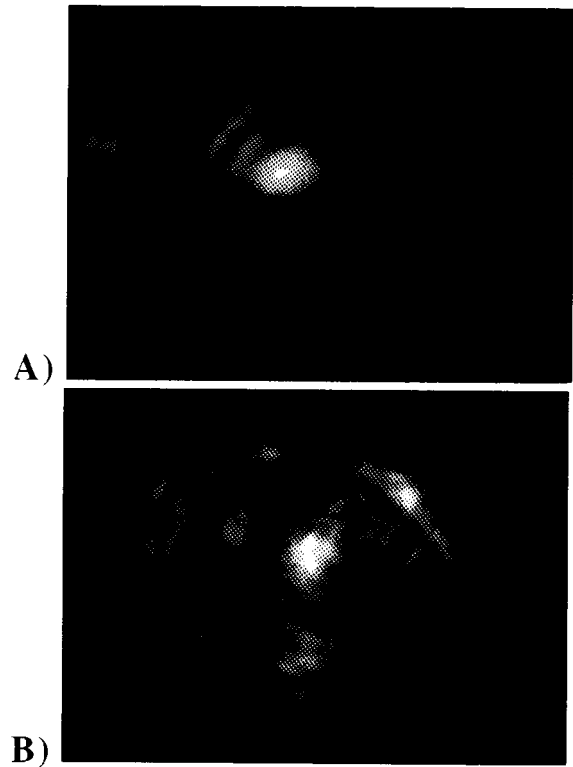


FIG. 6. (a) Image of focal spot of probe beam in vacuum ( $1/e^2$  diam  $\sim 9 \mu\text{m}$ ). (b) Image of the guided probe beam waist at channel exit [same scale as in (a)].

We have also profiled the exit mode structure of the probe pulse during this interaction by imaging the focal spot with a microscope objective onto a CCD array. These images were obtained by adjusting the axial position of the array so that the lens imaged the exit of the channel. A profile of the mode structure at the channel exit is displayed in Fig. 6. The focal spot (radius  $\sim 4.5 \mu\text{m}$ ) of the probe beam without plasma [Fig. 6(a)] has a similar size as the profile of the probe beam waist at the exit of the high intensity laser-produced channel [Fig. 6(b)]. For Fig. 6(b) the channel exit was about 1.5 mm from the position of the vacuum best focus. The exit mode from the channel essentially maintains the original single mode structure (radius  $\sim 5 \mu\text{m}$ ) with surrounding diffraction rings and some lower intensity small scale structure. Without the focusing effect of the plasma waveguide the size of the probe beam is about  $300 \mu\text{m}$  at this position.

A waveguide structure must have been formed in the wake of the high intensity pump pulse since the Thomson scattering image of the probe beam was observed to be qualitatively similar to that of the pump beam. Although the pump pulse may be influenced by relativistic self-focusing, the probe pulse is too weak ( $P_{\text{probe}} \sim 10^{-2} P_{\text{crit}}$ ) to impart relativistic quiver velocities to the plasma electrons. The observed channel is also probably not caused by the outward propagation of a high density shock wave which has been used to produce a plasma waveguide in previous experiments.<sup>12</sup> The plasmas created in these experiments

should be relatively cold and the creation of a channel of diameter  $10\ \mu\text{m}$  using the hydrodynamic evolution of a plasma column requires at least several hundred picoseconds.

The formation of a plasma channel can be most easily attributed to the effects of ponderomotive forces associated with the intense pump laser pulse as it propagates through the plasma.<sup>16,33</sup> Initially, the pump laser pulse exerts a ponderomotive force on the plasma electrons and expels them radially. This sets up a large space charge force which propels the ions outward from the axis of propagation. After the passage of the pump pulse, the ions continue to drift radially at approximately the ion acoustic speed  $C_s = (ZT_e/m_i)^{1/2}$ , thus creating a plasma channel, where  $Z$  is the number of electrons per ion,  $T_e$  ( $T_i$ ) is the electron (ion) temperature, and  $m_e$  ( $m_i$ ) is the electron (ion) mass. The electron motion is described by the radial force balance,  $e\nabla_{\perp}\phi = m_e c^2 \nabla_{\perp}(1+a^2/2)^{1/2} + n_e^{-1} \nabla_{\perp} P_e$ , where  $e\nabla_{\perp}\phi$  is the space charge force,  $m_e c^2 \nabla_{\perp}(1+a^2/2)^{1/2}$  is the ponderomotive force,  $P_e = T_e n_e$  is the electron pressure,  $n_e$  is the electron density and  $a^2$  is related to the laser wavelength  $\lambda$  and intensity profile  $I$  by  $a^2 = 7.2 \times 10^{-19} \lambda^2 [\mu\text{m}] I [\text{W cm}^2]$ . This expression neglects the generation of plasma waves and assumes that the axial length of the laser pulse is large compared to the laser spot size and the plasma wavelength. In the linear regime, the ion motion is described by the continuity equation  $\partial \delta n_i / \partial t = -n_{i0} \nabla_{\perp} \cdot \mathbf{v}_{\perp}$  and the momentum equation  $m_i \partial \delta \mathbf{v}_{\perp} / \partial t = -Z e \nabla_{\perp} \phi$ , where  $\delta n_i$  and  $n_{i0}$  are the perturbed and ambient ion densities,  $\mathbf{v}_{\perp}$  is the radial ion velocity, and  $T_i \ll T_e$  is assumed. Combining the electron radial force balance, the ion continuity equation, and the ion momentum equation yields<sup>33</sup>

$$\left( \frac{\partial^2}{\partial t^2} - C_s^2 \nabla_{\perp}^2 \right) \frac{\delta n_i}{n_{i0}} \cong \frac{Z m_e}{4 m_i} \nabla_{\perp}^2 a^2, \quad (1)$$

assuming  $\delta n_i^2 / n_{i0}^2 \ll 1$ ,  $a^2 \ll 1$ , and an isothermal equation of state.

Equation (1) has been evaluated<sup>33</sup> for a nonevolving laser pulse of the form  $a^2 = a_0^2 f(\zeta) \exp(-2r^2/r_0^2)$ , with  $f = \sin^2(\pi\zeta/L)$  for  $0 \leq \zeta \leq L$  and  $f = 0$  otherwise, where  $\zeta = z - ct$ . The evolution of the density channel is shown in Fig. 7 for the illustrative parameters  $a_0 = 0.25$ ,  $r_0 = 10\ \mu\text{m}$ ,  $L = 120\ \mu\text{m}$ ,  $T_e = 100\ \text{eV}$ ,  $Z = 2$ ,  $m_i/m_e = 7300$ , and  $C_s/c = 2.3 \times 10^{-4}$ . Figure 7 indicates a maximum density depletion ( $\delta n_{i0}/n_{i0} \cong 0.47$ ) is reached at about 30 ps for the simulation parameters. Despite the simplifying assumptions used, these calculations clearly show that a short lived plasma channel can be created in the wake of a high intensity short pulse laser propagating through an underdense plasma—agreeing qualitatively with experimental results.

## V. MEASUREMENTS OF ACCELERATED ELECTRONS

High energy electrons produced in the SM-LWFA are measured by a magnetic spectrometer and plastic scintillator/photomultiplier detector. An energy scan is shown in Fig. 8. This is raw data showing the electron signal at a range of cutoff energy settings (1–30 MeV). The data points are the total relative number of electrons above the energy specified

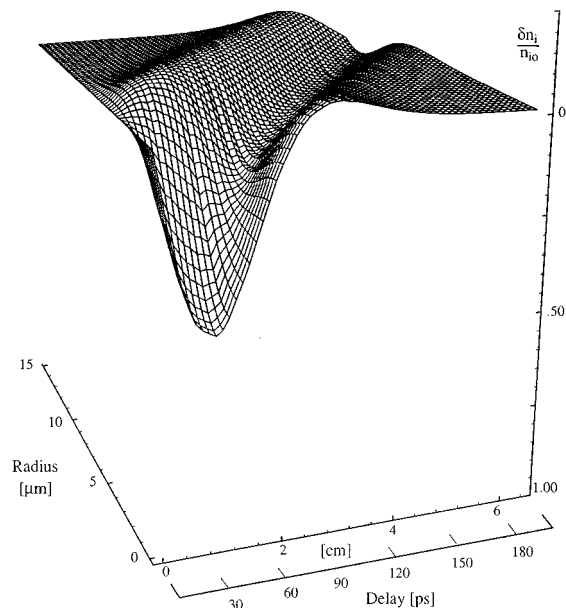


FIG. 7. Solution of Eq. (1) for parameters discussed in text. A region of plasma density depletion is produced approximately 30 ps after passage of the high intensity pulse.

on the  $x$  axis. The large fluctuations are believed to be shot-to-shot fluctuations because the low energy (500 keV–4 MeV) electron spectrum (measured using Kodak DEF x-ray films as shown in Fig. 9) shows a smooth, exponentially decreasing electron signal as a function of energy. The fluctuations did not correlate with fluctuations in energies ( $\sim 10\%$ ) of the laser. One possible explanation for the fluctuations is the growth of the plasma waves from the self-modulation and the forward Raman instabilities which are seeded from noise. The source of the background accelerated electrons may also contribute to the large fluctuations. A possible source of the background accelerated electrons other than from wave breaking is the interaction of backward Raman scattered light with the laser wakefield,<sup>19,20</sup> which is discussed in Sec. VI.

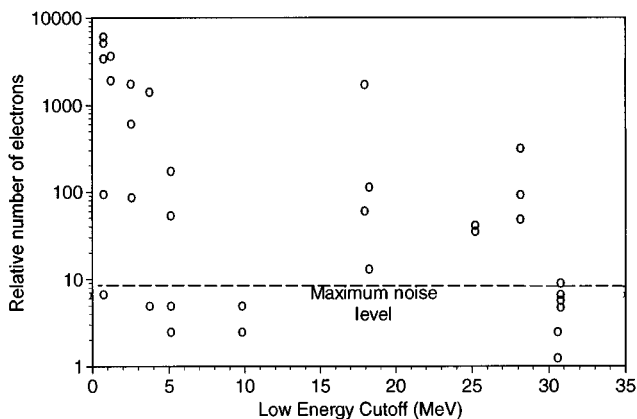


FIG. 8. The relative number of electrons above the cutoff energy of the spectrometer. The maximum noise level is the background noise level of the PMT. A signal above this level represents a clearly discernible signal from electrons striking the scintillator.

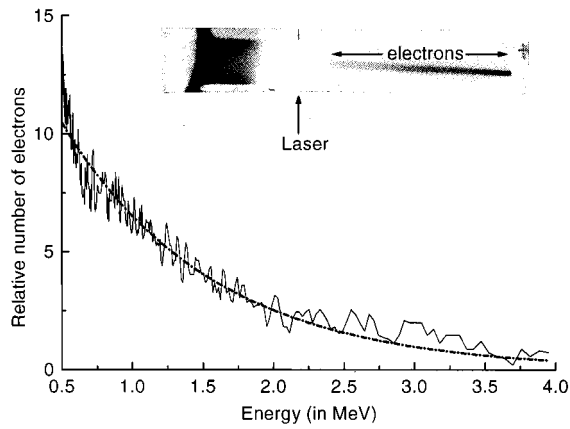


FIG. 9. Energy spectrum of accelerated electrons using direct exposure x-ray film. The dashed curve is an exponential fit to the data.

Concurrent with electron measurements we examined the spectrum of forward Raman scattered light. A typical spectrum is shown in Fig. 10 where strong nonlinearities of the plasma wave are obvious. As the plasma wave amplitude approaches or exceeds  $\delta n/n_0 = 1$ , the standard linear plasma wave theory breaks down. At this point the plasma wave “steepens” and harmonics of the plasma wave frequency became significant.<sup>6-8,36,37</sup> The presence of these plasma wave harmonics is readily apparent in the scattered spectrum as higher orders of the anti-Stokes line. The comparable amplitudes of the different order anti-Stokes lines in Fig. 10 indicate the presence of large plasma density modulations. Also, there is no indication of line broadening in the FRS spectra. The width of the first-order anti-Stokes line shown in Fig. 10 is the same as those we observed in the linear plasma wave regime (where only the first-order anti-Stokes line is observed). This indicates that although the wave has steepened, it has not begun to break as was observed by Modena *et al.* and Umstadter *et al.* at higher powers.<sup>7,8</sup>

The correlation of second-order anti-Stokes signal to electron production has been studied. For these experiments, the electron spectrometer measured the number of electrons with greater than 1 MeV of energy. For each laser shot the electron number and forward Raman scattering spectrum

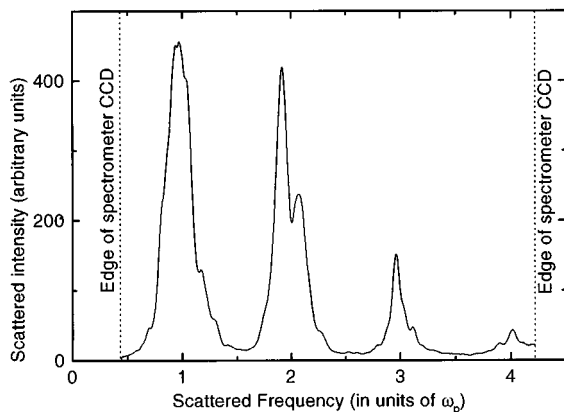


FIG. 10. Typical forward Raman scattering spectrum.

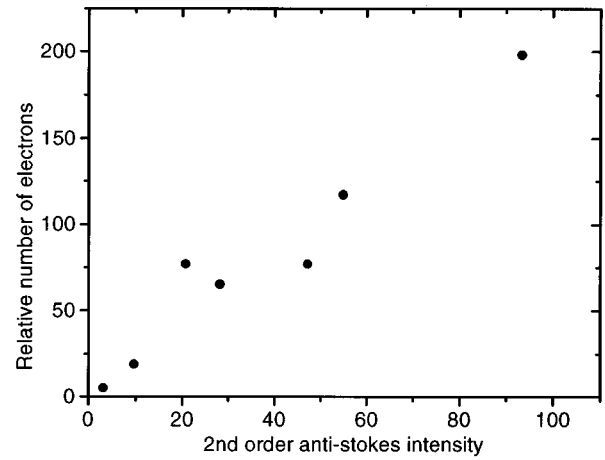


FIG. 11. The correlation between the second-order anti-Stokes signal and the number of high energy (>1 MeV) electrons

were recorded. The second-order anti-Stokes signal vs electron signal is shown in Fig. 11. A strong correlation between second-order anti-Stokes and electron signal was observed. This perhaps indicates that electrons are only accelerated from the background plasma as the plasma wave becomes nonlinear.

The profile of high energy (>1 MeV) electrons was recorded using Kodak DEF x-ray film as shown in Fig. 12. The beam profile shows a well collimated electron beam with a cone angle approximately half of the exit cone of the laser. The small divergence of the high energy electron beam indicates that it is well trapped by both the axial and radial wakefields of the plasma wave. There is also an absence of a hollow profile as observed by Umstadter *et al.*<sup>8</sup>

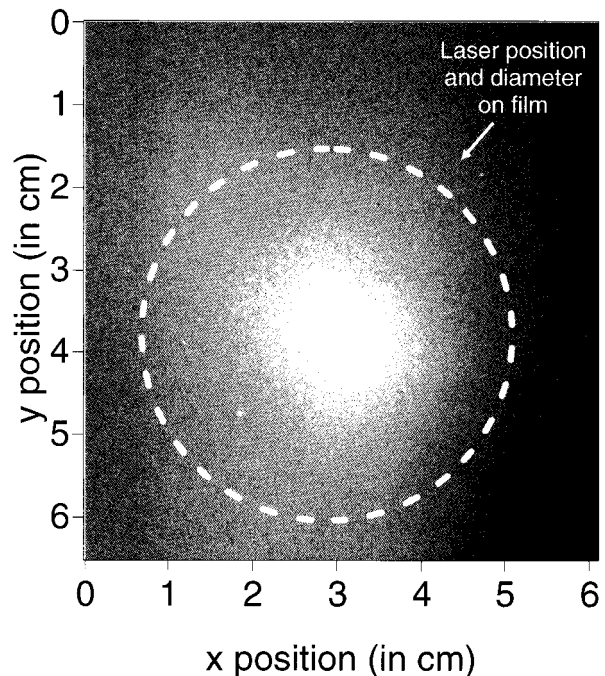


FIG. 12. Transverse profile of accelerated electrons as registered on film.

## VI. TRAPPING AND ACCELERATION OF PLASMA ELECTRONS

In principle, it is possible for a wakefield with sufficiently large amplitude to trap and accelerate cold plasma electrons. This corresponds to the limit of cold wave breaking. However, at lower wakefield amplitudes, some fraction of the cold plasma electrons can be trapped and accelerated by the wakefield if they are first pre-accelerated by some lower phase velocity wave. One potential candidate is backward Raman scattering (RBS), which produces a backward going light wave which beats against the pump light to drive a space charge wave with a slow phase velocity. Bertrand *et al.*<sup>19</sup> have reported Vlasov simulations of a two stage acceleration process in which electrons are first accelerated by RBS and then later accelerated to high energies by forward Raman scattering. Although their simulations were in the regime of laser fusion plasmas, an analogous process of two-stage acceleration is likely to occur in the SM-LWFA.

To investigate multi-stage acceleration, a one-dimensional model is used in which the various waves are specified analytically, and a large number of test particles are pushed in the prescribed fields.<sup>20</sup> The calculations are carried out in a frame moving at  $v_g = \beta_g c$  which is the group velocity for the pump laser pulse. The various waves are specified as functions of  $\psi = k_p(z - v_g t)$  with the laser pulse head at  $\psi = 0$  and the pulse tail at  $\psi = -L_p$ . The laser pump wave has a frequency  $\omega_0$ , wave number  $k_0$ , and amplitude  $a_0(\psi)$  with a maximum value  $a_{0m} = 1.0$ . The wakefield oscillates at  $\omega_p$  with an amplitude  $\phi_p$  (the space charge potential normalized to  $m_e c^2/e$ ), which grows over a few  $\lambda_p$  in the pulse to a maximum  $\phi_{p0} = E_z/E_0$ , where  $E_0 \approx 0.97 (n_e [\text{cm}^{-3}])^{1/2} \text{ V/cm}$ . The RBS light wave has frequency  $\omega_0 - \omega_p$  and wave number  $\approx -k_0$  and is assumed to grow and saturate very quickly at some point in the pump pulse. We have treated the instability heuristically by specifying a saturation amplitude  $a_{2m}$ , a saturation location  $\psi_R$  and a growth rate  $\gamma_R$ . Accompanying the RBS light wave is a RBS plasma wave of phase velocity  $v_p \approx \omega_p/2k_0 \ll c$  with a saturation amplitude  $\phi_{Rm}$ . Simulation particles are loaded at rest in the lab frame with different initial positions  $\psi_i$  in front of the laser pulse. The equation of motion is integrated in time out to  $\tau = \omega_p t = \tau_{\text{max}}$  for each particle. Electrons which are not trapped by the wakefield slip out through the back of the laser pulse.

Typical simulation parameters are  $\omega_0/\omega_p = 15$ ,  $a_{0m} = 1$ ,  $L_p = 100$ , and  $\tau_{\text{max}} = 600$ . These are representative of the NRL experiment. Figure 13(a) is a phase space plot showing  $\gamma\beta_z$  vs  $\Psi$  for a case with a moderate wakefield amplitude ( $\phi_{p0} = 0.4$ ), and a low saturation amplitude for the RBS instability ( $a_{2m} = 0.017$  and  $\phi_{Rm} = 0.0011$ ). Here, some of the electrons are quasi-trapped with energies of a few MeV and continue to slip back through the wakefield. Figure 13(b) shows that when  $\phi_{p0}$  is raised to 0.5, some electrons are trapped and accelerated to a much higher energy ( $\sim 50 \text{ MeV}$ ). However, if  $\phi_{p0}$  is reduced to 0.3, there is no trapping, and electron energies remain well below 1 MeV. This result is consistent with the energies exceeding 30 MeV which have been seen in the NRL experiments. Since modest changes in the wakefield amplitude (or other wave ampli-

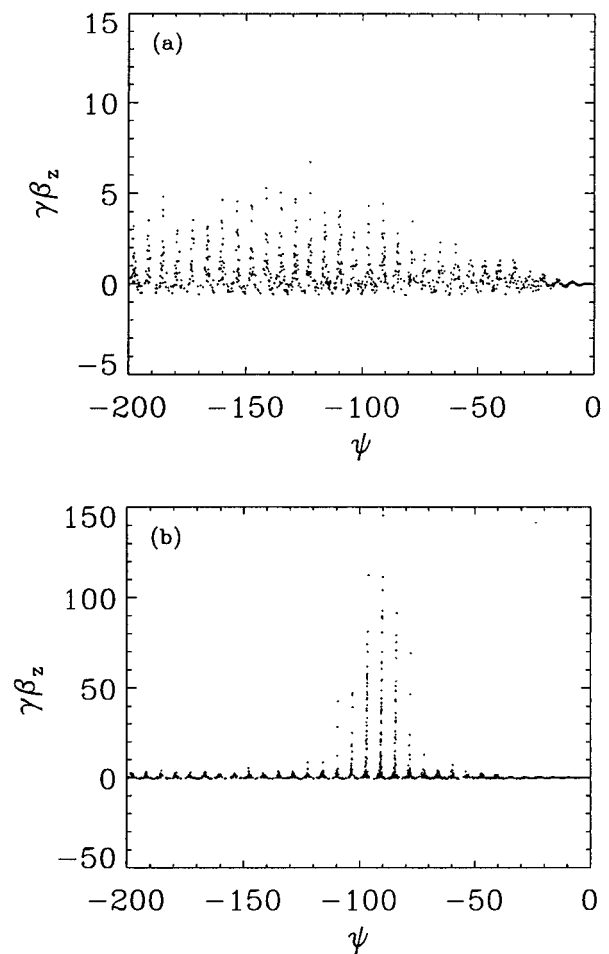


FIG. 13. Trapping of background plasma electrons by the interaction of the RBS plasma wave and the wakefield generated by the pump laser which extends from  $\psi = -100$ – $0$ , with wakefield amplitude: (a)  $\phi_{p0} = 0.4$ , (b)  $\phi_{p0} = 0.5$ . Note the tenfold difference in the vertical scale between (a) and (b).

tudes) can change the electron energy spectrum dramatically, one would expect substantial shot-to-shot variation in the experiment if operating near the threshold for substantial electron acceleration. This too is consistent with experimental results.

## VII. CONCLUSIONS

Coherent Thomson scattering of a picosecond probe laser was used to measure the time evolution of plasma wakefields produced by a high intensity laser pulse ( $7 \times 10^{18} \text{ W cm}^{-2}$ ) in an underdense hydrogen (or helium) plasma ( $n_e \approx 10^{19} \text{ cm}^{-3}$ ) in the self-modulated laser wakefield accelerator configuration. Large amplitude plasma wakefields are observed to last for less than 5 ps. Ion acoustic waves, generated by the decay of the plasma wakefield, were measured to have a duration of approximately 50 ps. These observations are consistent with the decay of large amplitude plasma waves due to the modulational instability and the enhancement of the scattered signal from possible plasma channel formation.

A plasma channel was observed to be formed behind the relativistically self-guided, subpicosecond, 2 TW pump laser

pulse in the gas jet plasma. The channel is probably produced from the radial expulsion of plasma ions due to charge separation created in the displacement (or cavitation) of plasma electrons by the large ponderomotive force of the laser. Using Thomson scattering diagnostics and mode structure measurements, a trailing, frequency doubled probe laser pulse is observed to be guided throughout the length of this channel for about 20 Rayleigh lengths—approximately equal to the propagation length of the self-guided pump laser pulse through the entire length of the gas jet plasma ( $\sim 2$  mm).

High energy electrons (up to 30 MeV) have been measured in the self-modulated laser wakefield accelerator using a 2.5 TW laser pulse and a high sensitivity, scintillator coupled to PMT detector. Highly nonlinear plasma waves have been detected using forward Raman scattering as a plasma diagnostic and a correlation between the nonlinear plasma waves and electron signal has been observed. The energy spectrum of accelerated electrons up to 4 MeV was recorded using direct exposure x-ray film. The transverse profile of the accelerated electrons was observed to be well confined within the exit divergence cone of the drive laser.

Simulation results have been presented to demonstrate a two-stage acceleration process that could self-trap and accelerate background plasma electrons to high energies. The slow phase velocity space charge wave generated by RBS preheats plasma electrons such that they can become trapped and accelerated by the laser wakefield. Simulations showed that this two-stage trapping mechanism is very sensitive to the wakefield amplitude and may be the source of shot-to-shot fluctuations observed in the production of high energy electrons in the experiment.

## ACKNOWLEDGMENTS

The authors would like to thank J. Grun, and A. Fisher for useful discussions and L. Daniels and K. Evans for technical assistance.

This work was supported by the Office of Naval Research and the U.S. Department of Energy.

- <sup>1</sup>E. Esarey, P. Sprangle, J. Krall, and A. Ting, *IEEE Trans. Plasma Sci.* **PS-24**, 252 (1996).
- <sup>2</sup>T. Tajima and J. M. Dawson, *Phys. Rev. Lett.* **43**, 267 (1979); P. Sprangle, E. Esarey, A. Ting, and G. Joyce, *Appl. Phys. Lett.* **53**, 2146 (1988).
- <sup>3</sup>P. Sprangle, E. Esarey, J. Krall, and G. Joyce, *Phys. Rev. Lett.* **69**, 2200 (1992).
- <sup>4</sup>T. M. Antonsen and P. Mora, *Phys. Rev. Lett.* **69**, 2204 (1992); N. E. Andreev, L. M. Gorbunov, V. I. Kirsanov, A. A. Pogosova, and R. R. Ramazashvili, *JETP Lett.* **55**, 571 (1992); W. B. Mori, C. D. Decker, D. E. Hinkel, and T. Katsouleas, *Phys. Rev. Lett.* **72**, 1482 (1994); E. Esarey, J. Krall, and P. Sprangle, *ibid.* **72**, 2887 (1994).
- <sup>5</sup>J. Krall, A. Ting, E. Esarey, and P. Sprangle, *Phys. Rev. E* **48**, 2157 (1993); E. Esarey, P. Sprangle, J. Krall, A. Ting, and G. Joyce, *Phys. Fluids B* **5**, 2690 (1993).
- <sup>6</sup>C. A. Coverdale, C. B. Darrow, C. D. Decker, W. B. Mori, K. C. Tseng, K. A. Marsh, C. E. Clayton, and C. Joshi, *Phys. Rev. Lett.* **74**, 4659 (1995).
- <sup>7</sup>A. Modena, Z. Najmudin, A. E. Dangor, C. E. Clayton, K. A. Marsh, C. Joshi, V. Malka, C. B. Darrow, C. Danson, D. Neely, and F. N. Walsh, *Nature* **377**, 606 (1995); 100 MeV electron detection recently reported by E. Clayton, *7th Workshop on Advanced Accelerator Concepts*, Lake Tahoe, California, 12–18 October 1996 (American Institute of Physics, Woodbury, NY, in press).
- <sup>8</sup>D. Umstadter, S.-Y. Chen, A. Maksimchuk, G. Mourou, and R. Wagner, *Science* **273**, 472 (1996).

- <sup>9</sup>C. I. Moore, K. Krushelnick, A. Ting, C. Manka, H. R. Burris, R. Fischer, M. Baine, E. Esarey, P. Sprangle, and R. Hubbard, in Ref. 7.
- <sup>10</sup>K. Nakajima, D. Fisher, T. Kawakubo, H. Nakanishi, A. Ogata, Y. Kato, Y. Kitagawa, R. Kodama, K. Mima, H. Shiraga, K. Suzuki, K. Yamakawa, T. Zhang, Y. Sakawa, T. Shoji, Y. Nishida, N. Yugami, M. Downer, and T. Tajima, *Phys. Rev. Lett.* **74**, 4428 (1995).
- <sup>11</sup>J. R. Marques, J. P. Geindre, F. Amiranoff, P. Audebert, J. C. Gauthier, A. Antonetti, and G. Grillon, *Phys. Rev. Lett.* **19**, 3566 (1996); C. W. Siders, S. P. Le Blanc, D. Fisher, T. Tajima, and M. C. Downer, *ibid.* **19**, 3570 (1996).
- <sup>12</sup>H. M. Milchberg, T. R. Clark, C. G. Durfee III, T. M. Antonsen, and P. Mora, *Phys. Plasmas* **3**, 2149 (1996).
- <sup>13</sup>S. Jackel, R. Burris, J. Grun, A. Ting, C. Manka, K. Evans, and J. Kosakowski, *Opt. Lett.* **20**, 1086 (1995).
- <sup>14</sup>A. Zigler, Y. Ehrlich, C. Cohen, J. Krall, and P. Sprangle, *J. Opt. Soc. Am. B* **13**, 68 (1996); Y. Ehrlich, C. Cohen, A. Zigler, J. Krall, P. Sprangle, and E. Esarey, *Phys. Rev. Lett.* **77**, 4816 (1996).
- <sup>15</sup>A. B. Borisov, A. V. Borovskiy, V. V. Korobkin, A. M. Prokhorov, O. B. Shiryayev, X. M. Shi, T. S. Luk, A. McPherson, J. C. Solem, K. Boyer, and C. K. Rhodes, *Phys. Rev. Lett.* **68**, 2309 (1992); A. Sullivan, H. Hamster, S. P. Gordon, R. W. Falcone, and H. Nathel, *Opt. Lett.* **19**, 1544 (1994); P. Monot, T. Auguste, P. Gibbon, F. Jakob, G. Mainfray, A. Dulieu, M. Louis-Jacquet, G. Malka, and J. L. Miquel, *Phys. Rev. Lett.* **74**, 2953 (1995).
- <sup>16</sup>K. Krushelnick, A. Ting, C. I. Moore, H. R. Burris, E. Esarey, P. Sprangle, and M. Baine, "Plasma channel formation and guiding during high intensity short pulse laser plasma experiments," submitted to *Phys. Rev. Lett.*
- <sup>17</sup>P. Sprangle, C. M. Tang, E. Esarey, *IEEE Trans. Plasma Sci.* **PS-15**, 145 (1987).
- <sup>18</sup>G. Z. Sun, E. Ott, Y. C. Lee, and P. Guzdar, *Phys. Fluids* **30**, 526 (1987); W. B. Mori, C. Joshi, J. M. Dawson, D. W. Forslund, and J. M. Kindel, *Phys. Rev. Lett.* **60**, 1298 (1988); P. Sprangle, A. Zigler, and E. Esarey, *J. Appl. Phys.* **58**, 346 (1991); G. Bonnaud, H. S. Brandi, C. Manus, G. Mainfray, and T. Lehner, *Phys. Plasmas* **1**, 968 (1994); K. Krushelnick, A. Ting, A. Fisher, C. Manka, H. R. Burris, and E. Esarey, *Phys. Rev. Lett.* **75**, 3681 (1995); C. Decker, W. B. Mori, K. C. Tseng, and T. Katsouleas, *Phys. Plasmas* **3**, 2047 (1996).
- <sup>19</sup>Bertrand, A. Ghizzo, S. J. Karttunen, T. J. H. Pattikangas, R. R. E. Salomaa, and M. Shoucri, *Phys. Rev. E* **49**, 5656 (1994); Bertrand, A. Ghizzo, S. J. Karttunen, T. J. H. Pattikangas, R. R. E. Salomaa, and M. Shoucri, *Phys. Plasmas* **2**, 3115 (1995).
- <sup>20</sup>R. F. Hubbard, P. Sprangle, E. Esarey, A. Ting, H. R. Burris, C. I. Moore, and K. Krushelnick, *Bull. Am. Phys. Soc.* **41**, 1602 (1996).
- <sup>21</sup>D. Umstadter, J. K. Kim, and E. Dodd, *Phys. Rev. Lett.* **76**, 2073 (1996).
- <sup>22</sup>E. Esarey, R. Hubbard, W. Leemans, A. Ting, and P. Sprangle, "Electron injection into plasma wakefields by colliding laser pulses," submitted to *Phys. Rev. Lett.* (1996); E. Esarey, R. Hubbard, W. Leemans, A. Ting, and P. Sprangle, in Ref. 7.
- <sup>23</sup>P. Maine, D. Strickland, P. Bado, M. Pessot, and G. Mourou, *IEEE J. Quantum Electron.* **QE-24**, 398 (1988); M. D. Perry and G. Mourou, *Science* **264**, 917 (1994).
- <sup>24</sup>P. Monot, T. Auguste, L. A. Lompre, G. Mainfray, and C. Manus, *J. Opt. Soc. Am. B* **9**, 1579 (1992); W. P. Leemans, C. E. Clayton, W. B. Mori, K. A. Marsh, P. K. Kaw, A. Dyson, C. Joshi, and J. M. Wallace, *Phys. Rev. A* **46**, 1091 (1992).
- <sup>25</sup>W. Wood, C. Siders, and M. Downer, *Phys. Rev. Lett.* **67**, 3523 (1991); E. Esarey, G. Joyce, P. Sprangle, *Phys. Rev. A* **44**, 3908 (1991).
- <sup>26</sup>A. Ting, K. Krushelnick, C. I. Moore, H. R. Burris, E. Esarey, J. Krall, and P. Sprangle, *Phys. Rev. Lett.* **77**, 5377 (1996).
- <sup>27</sup>S. P. Le Blanc, M. C. Downer, R. Wagner, S. Y. Chen, A. Maksimchuk, G. Mourou, and D. Umstadter, *Phys. Rev. Lett.* **77**, 5381 (1996).
- <sup>28</sup>D. M. Villeneuve, H. A. Baldis, J. E. Bernard, and R. Benesch, *J. Opt. Soc. Am. B* **8**, 895 (1991).
- <sup>29</sup>F. Martin, T. W. Johnston, and E. Ebrahim, *Phys. Rev. Lett.* **55**, 1651 (1985); C. E. Clayton, C. Joshi, C. Darrow, and D. Umstadter, *ibid.* **55**, 1652 (1985).
- <sup>30</sup>R. E. Slusher and C. M. Surko, *Phys. Fluids* **23**, 472 (1980).
- <sup>31</sup>P. Mora, D. Pesme, A. Heron, G. Laval, and N. Silvestre, *Phys. Rev. Lett.* **61**, 1611 (1988); D. Pesme, S. J. Karttunen, R. R. E. Salomaa, G. Laval, and N. Silvestre, *Lasers Part. Beams* **6**, 199 (1988).
- <sup>32</sup>F. Amiranoff, L. Laberge, J. R. Marques, F. Moulin, E. Fabre, B. Cros, G. Mattiasson, P. Benheiri, F. Jacquet, J. Meyer, Ph. Mine, C. Stenz, and P. Mora, *Phys. Rev. Lett.* **68**, 3710 (1992); F. Moulin, F. Amiranoff, L.

- Laberge, J. R. Marques, B. Cros, G. Matteussent, D. Bernard, F. Jacquet, Ph. Mine, A. Specke, C. Stenz, and P. Mora, *Phys. Plasmas* **1**, 1318 (1994).
- <sup>33</sup>E. Esarey, A. Ting, K. Krushelnick, C. I. Moore, M. Baine, and P. Sprangle, in Ref. 7.
- <sup>34</sup>T. E. Glover, T. D. Donnelly, E. A. Lipman, A. Sullivan, and R. W. Falcone, *Phys. Rev. Lett.* **73** 78 (1994); W. J. Blyth, S. G. Preston, A. A. Offenberger, M. H. Key, J. S. Wark, Z. Najmudin, A. Modena, A. Djaoui, and A. E. Dangor, *ibid.* **74**, 554 (1995).
- <sup>35</sup>J. A. Stamper, R. H. Lehmberg, A. Schmitt, M. J. Herbst, F. C. Young, J. H. Gardner, and S. P. Obenschain, *Phys. Fluids* **28**, 2563 (1985); P. E. Young, H. A. Baldis, T. W. Johnston, W. L. Kruer, and K. G. Estabrook, *Phys. Rev. Lett.* **63**, 2812 (1989); A. Ting, K. Krushelnick, H. R. Burris, A. Fisher, C. Manka, and C. I. Moore, *Opt. Lett.* **21**, 1096 (1996).
- <sup>36</sup>P. Sprangle, E. Esarey, and A. Ting, *Phys. Rev. Lett.* **64**, 2011 (1990).
- <sup>37</sup>D. Umstadter, R. Williams, C. Clayton, and C. Joshi, *Phys. Rev. Lett.* **59**, 292 (1987).